Journal of Oceanology and Limnology

https://doi.org/10.1007/s00343-023-3103-8

Paleosalinity reconstruction in offshore lacustrine basins based on elemental geochemistry: a case study of Middle-Upper Eocene Shahejie Formation, Zhanhua Sag, Bohai Bay Basin*

Long SUN[1, 2], Shenghe WU[1, 2, **], Dali YUE[1, 2], Wenfu CUI[3]

[1] *National Key Laboratory of Petroleum Resources and Engineering*, *China University of Petroleum* (*Beijing*), *Beijing 102249*, *China*

[2] *College of Geosciences*, *China University of Petroleum* (*Beijing*), *Beijing 102249*, *China*

[3] *Shengli Oil Production Plant*, *Shengli Oilfield Company*, *SINOPEC*, *Dongying 257400*, *China*

Received Jun. 2, 2023; accepted in principle Jul. 23, 2023; accepted for publication Oct. 8, 2023

Abstract Salinity is a crucial property of water body and is essential for the restoration of paleoecology and paleoenvironment. However, the theoretical method of application of elemental geochemical proxies to paleosalinity reconstruction is still underdeveloped. Moreover, accurate determination and reconstruction of paleosalinity and its variation in an offshore lacustrine basin have been extremely challenging thus far. This study presents detailed elemental geochemical investigations from the Zhanhua Sag in the southern Bohai Bay Basin to reconstruct the salinity variation in the Paleogene Eocene Shahejie Formation (50.8–33.9 Ma). Based on the variation of strontium barium ratio (Sr/Ba) and boron gallium ratio (B/Ga), we determined three typical salinity types of water body: salty water (Sr/Ba>0.5, B/Ga>6), brackish water (0.2<Sr/Ba<0.5, 3<B/Ga<6), and fresh water (Sr/Ba<0.2, B/Ga<3), after eliminating carbonate-sourced strontium (Sr). The salinity values following Couch's paleosalinometer ranged from 3.1 to 11.9, reflecting the overall characteristics of oligohaline (0.5<salinity value<5) to mesohaline (5<salinity value<18) brackish water. All proxies yielded similar trends in paleosalinity variation, demonstrating a clear trend of rising and then declining from 50.8 Ma to 33.9 Ma. We considered that the B/Ga ratio had the highest reliability and resolution in determining the salinity types of water body in the study area. The environmental factors causing paleosalinity variation were also thoroughly analysed based on the temporal relationship among the salinity types of watermasses, paleoclimate characteristics from pollen records, and marine transgression events from marine fossils. Our research established a model of paleoclimatic and eustatic mechanisms to explain paleosalinity variation, providing reasonable and integral driving forces for the salinity variation of all offshore lacustrine basins.

Keyword: paleosalinity; paleoclimate; Zhanhua Sag; Middle-Upper Eocene; Shahejie Formation

1 INTRODUCTION

Paleosalinity proxies are of immense significance in reconstructing paleoclimates and restoring sedimentary environments (Ye et al., 2016; Wei et al., 2021). In recent years, extensive research efforts in shale oil and gas exploration have shed new light on the role of paleosalinity conditions in organic matter enrichment (Hudec et al., 2006; Tao et al., 2015). Particularly, there has been a deeper understanding of hydrocarbon generation mechanisms in saline environments (Edgell, 1996; Ma et al., 2000). This understanding has significantly enhanced the evaluation of resource potential in saline basins such as the Bohai Bay Basin in China (Jiang et al., 2022). Accurate reconstruction of paleosalinity not only

* Supported by the National Natural Science Foundation of China (No. 42272110)

** Corresponding author: reser@cup.edu.cn

serves as a research foundation for sedimentology but also plays a vital role in the study of oil and gas resource formation and distribution (Sun et al., 2022a). However, historically, research in sedimentary geochemistry has primarily focused on restoring paleoenvironmental conditions, such as redox and primary productivity, while the exploration of paleosalinity indicators has remained relatively nascent (Wei et al., 2018, 2021). It is therefore imperative to apply various indicators for paleosalinity analysis to address this research gap.

While the rock characteristics and paleogeographic background can provide insights into whether the water is marine saline or fresh water from terrestrial enclosed lake basins (Wei and Algeo, 2020), there is typically little uncertainty in such cases. However, in the context of ancient sedimentary formations deposited in coastal terrestrial settings or marginal-marine, water salinity is influenced by a combination of regional climate (Ye et al., 2016) and sea level changes (Wei et al., 2018). As a result, it becomes crucial to determine the secular variation or long-term average paleosalinity conditions to understand the complex dynamics at play. In addition to the rock assemblage characteristics, fossil assemblages play a crucial role in paleosalinity analysis (Wei and Algeo, 2020). Various faunal and floral groups have been employed, including the abundance of sporopollen fossils and facies fossils such as ostracods and dinoflagellates (Wei and Algeo, 2020). However, it's important to note that fossil-based techniques are only applicable when there is fossil deposition and preservation. In many instances, fossil assemblages can only provide a rough estimation of salinity levels.

Compared to traditional methods of analysing mineral composition and fossil facies, geochemical proxies play an essential role in reconstructing paleoenvironments. While various element geochemical proxies of sedimentary rocks have been used for the paleoenvironmental restoration of marine and lacustrine systems for a long time, one of the parameters that is difficult to evaluate is paleosalinity (Harder, 1970; Zhang et al., 2017; Wei et al., 2018; Sun et al., 2022b). Since the distribution of trace elements in different sedimentary environments was revealed, several methods, such as the boron (B) content (Walker and Price, 1963; Walker, 1968), strontium barium ratio (Sr/Ba) (Wang et al., 1979), boron gallium ratio (B/Ga) (Qian and Shi, 1982) and carbon and oxygen isotopes ($\delta^{13}C$ and $\delta^{18}O$) (Degens et al., 1957), have been proposed successively to reconstruct paleosalinity. However, with the widespread application of the aforementioned methods in ancient marine and lacustrine systems, sedimentologists have found numerous interferences that occur when directly using the element concentrations in rocks, such as the influence of provenance and diagenesis (Ye et al., 2016; Wei and Algeo, 2020). Furthermore, substantial efforts have been made to rectify the detrital background concentrations (inherited B and carbonate-sourced strontium (Sr)) (Ye et al., 2016; Wei and Algeo, 2020) and differential authigenic adsorption (equivalent B content, Adams' paleosalimeter and Couch's paleosalimeter) (Price and Walker, 1963; Adams et al., 1965; Couch, 1971). Thus, to date, paleosalinity analysis based on corrected elemental proxies is a promising approach and has been widely used by sedimentary scholars (Wei and Algeo, 2020; Sun et al., 2022b; Wei et al., 2022).

The Zhanhua Sag, a major hydrocarbon province with rich, cumulative and proven oil reserves in the Jiyang Depression, Bohai Bay Basin and containing dense accumulations of the Eocene lacustrine source rocks (Shi et al., 2005; Wei et al., 2018), is an ideal basin to explore paleosalinity variation and its formation mechanism. Nonetheless, long-term paleosalinity reconstruction records of the Middle-Late Eocene from the Zhanhua Sag are scarce due to the absence of reliable proxies in thick sedimentary sequences with complex variations in provenance composition (Cai et al., 2011; Wei and Algeo, 2020). While Wei et al. (2018) reconstructed the paleosalinity of the lower sub-member of the 3rd member of the Eocene Shahejie Formation ($Es3^{L}$) and suggest that marine incursions contributed to the increased salinity in this interval, there is currently a dearth of comprehensive analysis regarding the salinity of the entire Eocene Shahejie Formation in the Zhanhua Sag. Furthermore, research on the influence of paleoclimate on paleosalinity in this context is lacking. Therefore, reliable paleosalinity proxies are essential to further study the temporal variation in salinity and its driving forces, such as regional climate evolution, tectonic movement and global sea level changes during the Middle-Upper Eocene Shahejie Formation.

This study presents detailed geochemical evidence of the Zhanhua Sag in the southern Bohai Bay Basin to reconstruct paleosalinity variation and its change pattern in the Middle-Late Eocene period (~50.8–33.9 Ma). We analysed 71 samples from six

core wells and optimised element geochemical proxies for paleosalinity analysis, including Sr/Ba ratio, B/Ga ratio, and Couch's paleosalimeter. By eliminating the influence of Sr derived from carbonate sources, we conducted an analysis of ancient salinity and examined the impact of material sources and diagenesis on salinity indicators. In doing so, we determined the salinity range of the ancient water bodies within the studied layer, categorizing them as either fresh water, brackish water, or salty water. We combined these findings with the results of pollen-based paleoclimate reconstructions and the occurrence of marine invasion events to further understand the driving forces behind changes in ancient salinity.

2 GEOLOGICAL BACKGROUND

The Bohai Bay Basin is a Meso-Cenozoic hydrocarbon-bearing rift basin located in the eastern part of the North China Craton, extending approximately 440 km in the NW-SE direction and 1 050 km in the NE-SW direction (Liu et al., 2016; Zhu et al., 2019; Hua et al., 2021). It is bounded by five primary tectonic units: the Taihang Mountain uplift to the west, the Yanshan fold belt to the north, the Jiaodong uplift and Liaodong uplift to the east and the Luxi uplift to the south, adjacent to the Tanlu Fault Zone (Liu et al., 2021; Zhu et al., 2022) (Fig.1a). The Bohai Bay Basin comprises several NE-trending secondary tectonic basins from west to east, including the Lingqing Depression, Jizhong Depression, Huanghua Depression, Jiyang Depression, Bozhong Depression, Liaodong Bay Depression, and Liaohe Depression, which collectively form a complex series of rift basins (Fig.1a). The Jiyang Depression, which is one of the four major oil-bearing depressions in the Bohai Bay Basin, is further subdivided by a series of small sags and uplifts (Zhang et al., 2020).

The Zhanhua Sag is a WE-trending rift located in the southeast of the Bohai Bay Basin and northeast of the Jiyang Depression, with an area of approximately 3 600 km² (Li et al., 2017; Ning et al., 2017; Liu et al., 2020b) (Fig.1a–b). The Zhanhua Sag is one of the four major hydrocarbon-rich sags within the Jiyang Depression, connected to the Yihezhuang Uplift and Chengdong Uplift in the north and adjacent to the Chezhen Sag, with the Gudao Uplift to the east and bound to the south by the Chenjiazhuang Uplift (Li et al., 2021, 2022). The sag is a hydrocarbon-rich, half-graben rift in the Bohai Bay Basin, with a series of well-developed northeast and east-west-trending faults (Fig.1c). The potential oil reserves of the sag have been estimated to be greater than 19.1×10^8 t by petroleum explorations (Li et al., 2017).

The Zhanhua Sag contains typical continental lacustrine clastic rocks with a total thickness of up to 10 000 m, including massive mudstone developed in the Paleogene (Zhu et al., 2019, 2022). The stratigraphic units in the Zhanhua Sag, from oldest to youngest, consist of the Kongdian Formation (Ek), Shahejie Formation (Es), and Dongying Formation (Ed), which mainly represent lacustrine facies. The Guantao Formation (Ng), Minghuazhen Formation (Nm), and Quaternary deposits (Q), including the Pingyuan Formation (Qp), are dominantly of fluvial facies (Wei et al., 2018) (Fig.1d–e). The Shahejie Formation is further divided into four members: the 4^{th} member (Es4), 3^{rd} member (Es3), 2^{nd} member (Es2), and 1^{st} member (Es1), from bottom to top. The focus of this study is the Middle-Upper Eocene Shahejie Formation (~50.80–33.90 Ma) (Wei et al., 2018), which can be subdivided into six sub-members from the bottom to top: the lower sub-member of the 4^{th} member ($Es4^L$), the upper sub-member of the 4^{th} member ($Es4^U$), the lower sub-member of the 3^{rd} member ($Es3^L$), the middle sub-member of the 3^{rd} member ($Es3^M$), the upper sub-member of the 3^{rd} member ($Es3^U$) and the lower sub-member of the 2^{nd} member ($Es2^L$) (Fig.1d). The Middle-Upper Eocene Shahejie Formation comprises fine-grained clastic deposits that gradually accumulated under shallow to deep lakes. It is mainly dominated by a set of dark grey mudstone in Es3, followed by silty mudstone, siltstone, sandstone, carbonate rock, evaporite and oil shale (Fig.1d).

3 MATERIAL AND METHOD

3.1 Sample and experiment

A total of 71 representative mudstone samples from the Middle-Upper Eocene Shahejie Formation were collected from six cored wells in different sub-members. The stratigraphic positions of the samples did not overlap and had similar source characteristics (Fig.1c). Within this interval, we analyzed these mudstone samples involving X-ray diffraction (XRD), X-ray fluorescence (XRF), and inductively coupled plasma atomic emission spectroscopy (ICP-AES) to determine the concentrations of clay minerals, major elements, and trace elements, respectively.

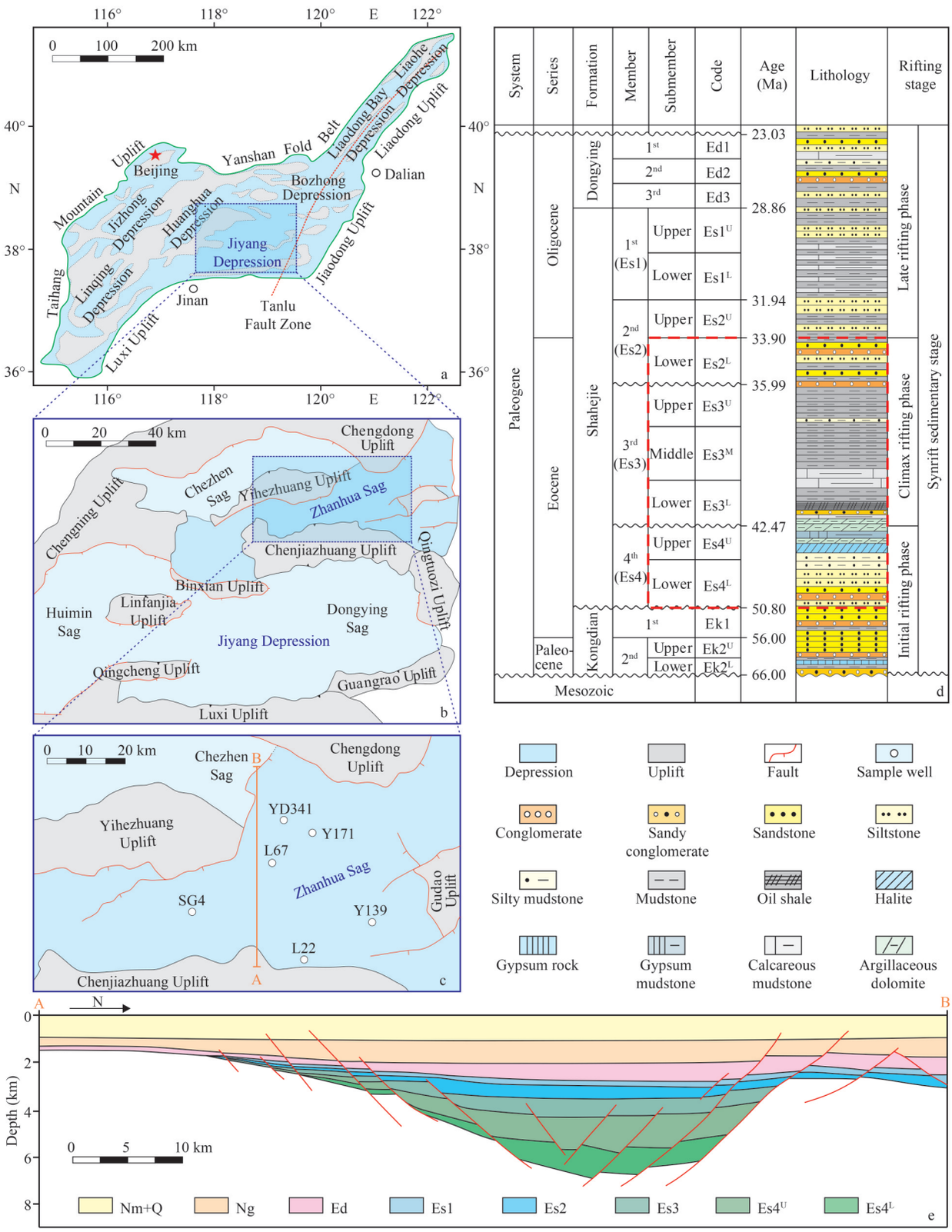

Fig.1 Location (a–c), stratigraphic units (d), and main structural units (e) of the Zhanhua Sag

a–c. location map and well locations of the Zhanhua Sag in the Jiyang Depression, Bohai Bay Basin, China; d. stratigraphic column depicting the lithostratigraphy of the study interval. The present study interval (Middle-Upper Eocene Shahejie Formation) is shown by the dashed red rectangle; e. structural features of the study area, see cross-section AB in panel c. Nm: Minghuazhen Formation; Q: Quaternary; Ng: Guantao Formation; Ed: Dongying Formation; Es1–Es4: the 1st to 4th members of the Shahejie Formation.

The core samples covered all sub-members and sub-sags in the study area and were obtained by cutting from fresh surfaces after removing the influence of mud stains.

Clay mineral compositions were quantitatively analyzed using XRD with a D8 Discover X-ray diffractometer at the SINOPEC Exploration and Production Research Institute of Shengli oilfield in Dongying, China. Prior to XRD analysis, the samples were ground into a powder with a particle size of <5 μm using an agate mortar and subsequently thoroughly dried at a low temperature of 40 °C for 48 h. Next, the dried powder samples were scanned using a D8 Discover X-ray diffractometer with Cu-K radiation, operating at 40 kV and 25 mA, with a range of 3°–70°, a step size of 0.02° and a scan rate of 10°/min. For each sample, the XRD pattern includes the natural air-dried (N), glycol-saturated (EG), and heated (T) diffractograms (Fig.2). The JADE 5.0 software was used to analyze the XRD patterns, identify the clay minerals present and calculate the relative weight percentages for clay minerals following the industry standard 'SYT 5163-2010' (National Energy Administration, 2010).

Semi-quantitative results of each clay mineral were estimated based on the heights and peak areas of the basal reflections for main clay minerals following "SYT 5163-2010" (National Energy Administration, 2010; Ye et al., 2016). The proportion of illite in illite/smectite mixed layers (I/S) was estimated based on "SY/T 5163-2010". In brief, the rate between the saddle and peak is first calculated for the peak of I/S from the EG diffractogram, and the ratio of illite to illite/smectite mixed layers (I/(I/S)) is then determined based on the peak areas of the glycol-saturated and heated diffractograms. Similarly, based on the saddle peak difference and I/(I/S) ratio, the percentage of smectite in the I/S can be obtained with an error of ±5%.

As with XRD analysis, researchers at the SINOPEC Exploration and Production Research Institute of Shengli Oilfield used ICP-AES and XRF to determine the contents of trace elements such as Sr, barium (Ba), B and gallium (Ga) and oxides such as K_2O and CaO, respectively. Tourmaline is a type of B-rich heavy mineral (normally >5 μm) that requires elimination as it affects the B content of the detrital minerals (Ye et al., 2016; Sun et al., 2022a). Therefore, to thoroughly disperse the minerals and eliminate the influence of tourmaline-derived B, the <5 μm fractions of samples were collected by gravity sedimentation following Stokes' Law. The final step of the pre-treatment involved acidifying approximately 20 mg of a dried powder sample in a Teflon container using a mixture of HF (40%) and HNO_3 (65%). The relative standard deviations (RSDs) for trace elements and oxides were <5% and 2%, respectively, in duplicate measurements.

3.2 Paleosalinity reconstruction method

The current study aims to restore the salinity conditions of a paleowater body by employing Sr/Ba, B/Ga, and Couch's paleosalimeter as elemental geochemical proxies. The ratios of Sr/Ba and B/Ga were applied to forecast the salinity characteristics of sediments, using distinct elemental ratio thresholds obtained from variances in the mobility of various

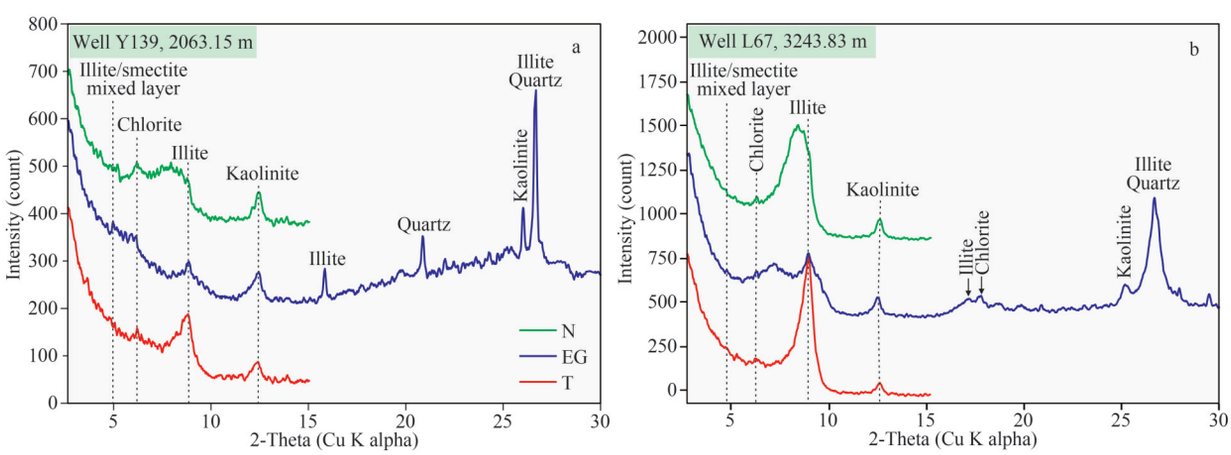

Fig.2 XRD patterns of two representative clay samples in the study interval

a. sample from 2 063.15 m in Well Y139 with partially regular illite/smectite mixed layer (I/S), illite, kaolinite, and chlorite; b. sample from 3 243.83 m in Well L67 with typical irregular illite/smectite mixed layer (I/S), illite, kaolinite, and chlorite. N: natural air-dried sample; EG: glycol-saturated sample; T: heated sample.

elements (Wang et al., 1979; Wei and Algeo, 2020).

One crucial challenge in utilizing the Sr/Ba ratio as a paleosalinity indicator is the potential interference of carbonate-sourced Sr, which can impact the signal from clay components. Pure carbonate rock sediments typically exhibit higher levels of Sr, with calcite content ranging from $1\,000\times10^{-6}$ to $3\,000\times10^{-6}$ and primary marine aragonite content ranging from $8\,000\times10^{-6}$ to $10\,000\times10^{-6}$ (Wei and Algeo, 2020). Consequently, the presence of carbonates in the sample may elevate the overall Sr/Ba ratio in comparison to the clay component. To address this issue, we carefully assessed the influence of Sr carbonate and established a maximum carbonate threshold for studying the Sr/Ba ratio within the given interval.

Based on the calibration results of salinity and Sr/Ba, B/Ga in the modern sedimentary system (Wei and Algeo, 2020), multiple indicators were employed to determine the optimal thresholds for different salinity levels in water bodies. Regarding the Sr/Ba ratio in sediment, values below 0.2 indicate the deposition of fresh water, while ratios ranging from 0.2 to 0.5 suggest brackish water deposition, and ratios exceeding 0.5 indicate salty water deposition. As for the B/Ga ratio in sediment, values below 3 indicate the deposition of fresh water, ratios between 3 and 6 suggest brackish water deposition, and ratios above 6 indicate salty water deposition.

In the paleosalinity reconstruction of this study, we used Couch's paleosalimeter to quantitatively calculate the salinity values of paleowater body. This method not only considers the adsorption of B by Illite, but also emphasizes the influence of kaolinite, montmorillonite, and other clay minerals (Qian and Shi, 1982). The results of B adsorption by different clay mineral types demonstrate that illite, smectite and kaolinite have a B absorption capacity ratio of 4∶2∶1. Furthermore, "Kaolinite B" (B_k) was utilized to further refine the B content (Couch, 1971). The B_k content in this study was calculated as follows:

$$B_k=B_t/(4X_i+2X_s+X_k), \quad (1)$$

where, X_i, X_s, and X_k denote the relative content (%) of illite, smectite, and kaolinite, respectively. Moreover, B_t was replaced by B^*. The paleosalinity value from Couch's equation (S_{pc}) was quantitatively calculated as follows:

$$\lg S_{pc}=(\lg B_k-0.11)/1.28. \quad (2)$$

4 RESULT

4.1 Carbonate-sourced Sr elimination

The use of adsorbed Sr during the deposition of clay minerals as a salinity-sensitive element is complicated by a large interfering term caused by the mixing of residual Sr from carbonate rocks with adsorbed Sr in experimental results (Wei and Algeo, 2020). Previous studies have indicated that pure carbonate rocks tend to contain higher concentrations of Sr compared to fine-grained clastic rocks, with concentrations ranging from approximately $1\,000\times10^{-6}$ to $3\,000\times10^{-6}$ in pure calcite and from $8\,000\times10^{-6}$ to $10\,000\times10^{-6}$ in aragonite (Wei and Algeo, 2020). However, inherited Sr in primitive carbonate minerals (Fig.3a, b, & e) may lead to higher measured Sr concentrations in some samples. The higher carbonate content of Sr can easily be mistaken for adsorbed Sr and used to calculate Sr/Ba ratios, ultimately increasing the Sr/Ba ratio in the sediments. Therefore, it is essential to eliminate all samples affected by residual Sr in carbonate rocks and establish carbonate thresholds for the study intervals (Wei and Algeo, 2020; Sun et al., 2022b).

In this study, the calcium oxide (CaO) content was used as a proxy for carbonate mineral content. Based on testing results, a positive correlation was observed between Sr and CaO (R^2=0.84) in the CaO threshold range >5% (Fig.4a). Thus, we used CaO=5% as the threshold for eliminating carbonate-sourced Sr by removing samples with CaO content below this threshold. Samples were screened accordingly, and those with CaO content less than 5% were presumed to contain inherited Sr and could not be used for paleosalinity reconstruction. Furthermore, some of the samples having <5% CaO also contain evident carbonate-sourced Sr. These samples fall into two groups: one group with $(250–700)\times10^{-6}$ Sr, and one with $>1\,000\times10^{-6}$ Sr. Samples that simultaneously meet CaO<5% and Sr<$1\,000\times10^{-6}$ are typical mudstone values unaffected by carbonate, and it is this group that should be used for paleosalinity analysis. The Sr/Ba ratio for samples with Sr content between 250×10^{-6} and 700×10^{-6} and CaO<5% falls within the range of 0 to 3. On the other hand, the Sr/Ba ratio for samples with Sr>$1\,000\times10^{-6}$ varies between 3 and 12, providing additional evidence of a significant presence of Sr derived from carbonates in the latter group of samples (Fig.4b).

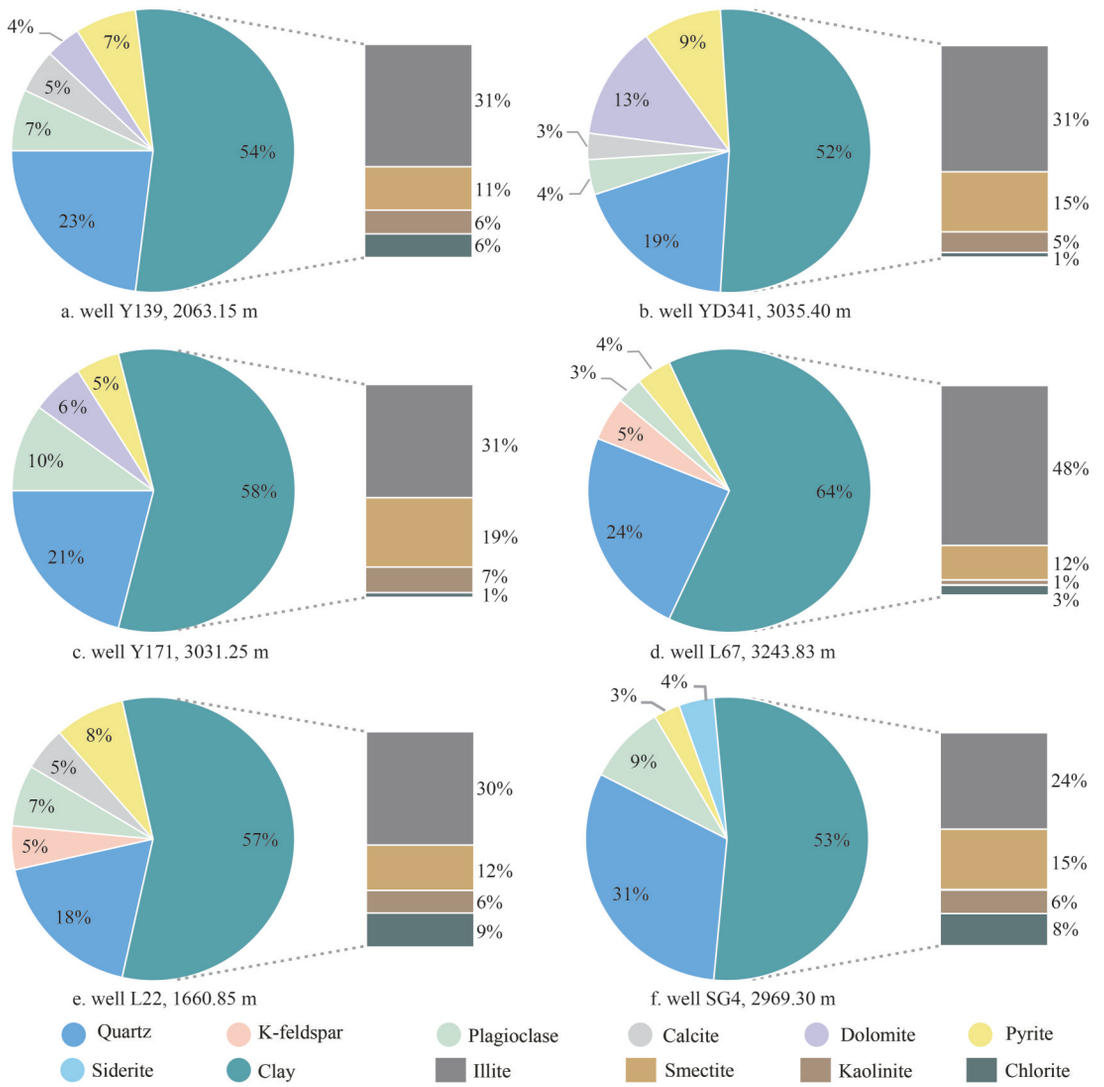

Fig.3 Pie chart of XRD analyses of six representative samples from different wells in the Zhanhua Sag

The pie chart on the left illustrates the proportion of minerals in the whole rock, and the bar chart on the right shows the percentage of clay minerals in the whole rock.

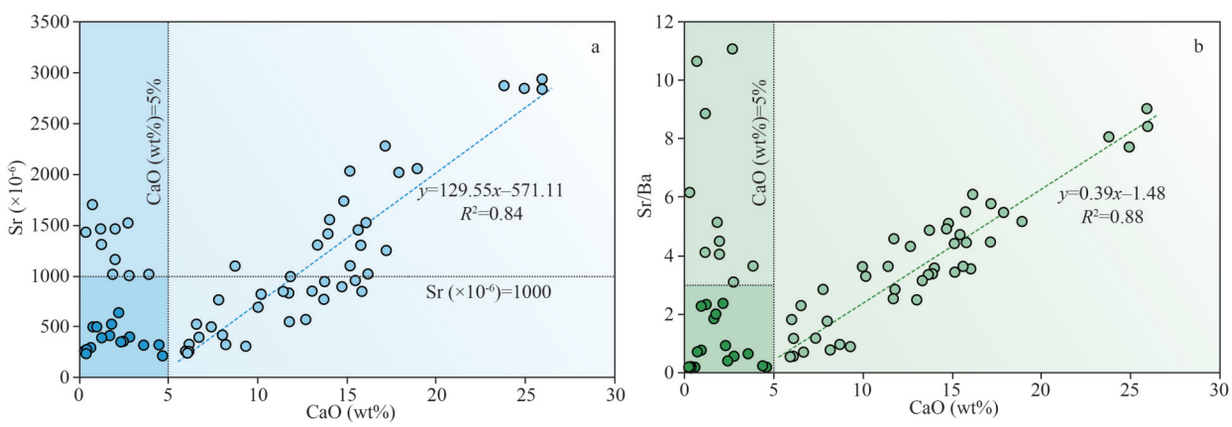

Fig.4 Threshold determination to screen out carbonate-sourced Sr in the study interval

a. Sr versus CaO; b. Sr/Ba versus CaO. Note the lack of correlations for CaO<5% and the strong positive correlations for CaO>5% in panels a and b. Data points with CaO>5% and Sr>1 000×10^{-6} represent carbonate-sourced Sr and should not be utilized for paleosalinity reconstruction purposes.

4.2 Sr/Ba ratio

We systematically analyzed 71 samples from the Zhanhua Sag, determining their Sr, Ba, B, Ga, and other elemental contents. Following the elimination of carbonate-sourced Sr, we established Sr-Ba cross-plots for 18 samples using the subset of sub-members with distinct color regions (Fig.5a). The study interval demonstrated ranges of Sr and Ba contents of (213.6–638.1)×10^{-6} (n=18), (167.0–1 550.0)×10^{-6} (n=18), respectively. The slope of the line connecting the sample points to the origin in the cross-plot represents the Sr/Ba ratios. Accordingly, we plotted histograms of their minimum, maximum and average values in different sub-members (Fig.5b). The elemental ratio histograms (Fig.5b) indicate that the highest value of Sr/Ba ratios was observed in $Es3^{L}$, while the lowest value was found in $Es2^{L}$. The Sr/Ba ratio of the entire Eocene Shahejie Formation study interval ranges from 0.16 to 2.37, with an average value of 0.9. Additionally, the ratios of these two elements displayed a trend of increasing and then decreasing throughout the Middle-Upper Eocene Shahejie Formation.

4.3 B/Ga ratio

Given the distinct behaviours of B and Ga during sedimentation, the B/Ga ratio has become a commonly employed indicator for ancient salinity levels. Notably, freshwater sediments exhibit higher Ga content compared to marine sediments (Potter et al., 1963), which stands in stark contrast to the aforementioned enrichment of B in saltier settings. Hence, marine environments typically feature higher B/Ga ratios than freshwater environments, making this ratio widely utilized as a paleosalinity proxy in numerous studies (Ye et al., 2016; Zhang et al., 2017; Wei et al., 2018).

In the Middle-Upper Eocene Shahejie Formation, the B mass fraction spans from 9.8×10^{-6} to 89.8×10^{-6}, with an average value of 43.9×10^{-6}. Conversely, the Ga content ranges from 2.1×10^{-6} to 16.7×10^{-6}, with an average of 6.7×10^{-6} (Fig.6a). Furthermore, the B content demonstrates an initial increase followed by a decrease from bottom to top (from $Es4^{L}$ to $Es2^{L}$). The B/Ga ratio range for the Middle-Upper Eocene Shahejie Formation is 2.4–11.6, with an average ratio of 6.9. It exhibits a similar systematic trend to the Sr/Ba ratios, increasing initially and subsequently declining gradually as indicated by the data from $Es4^{L}$ (3.2–6.7, average 5.0), $Es4^{U}$ (4.7–11.6, average 7.8), $Es3^{L}$ (5.1–11.1, average 8.5), $Es3^{M}$ (2.8–4.0, average 3.3), $Es3^{U}$ (3.1–4.4, average 3.9), and $Es2^{L}$ (2.4–3.0, average 2.8) (Fig.6b).

4.4 Couch's paleosalimeter

The XRD analysis of 71 samples yielded the relative proportions of different clay mineral fractions (Table 1; Fig.3). Based on these values and B content, the "Kaolinite B" and paleosalinity (S_{pc}) within the study interval were determined using equations 1 and 2, respectively, according to Couch's paleosalimeter. In this study, we assumed that the B content absorbed by clay minerals aligns with the findings of Couch, 1971. Therefore, equation 1 employs a 4∶2∶1 coefficient to represent the relative amount of B absorbed by illite, smectite and kaolinite, which is equivalent to the B content absorbed solely by kaolinite, referred to as the "Kaolinite B" content.

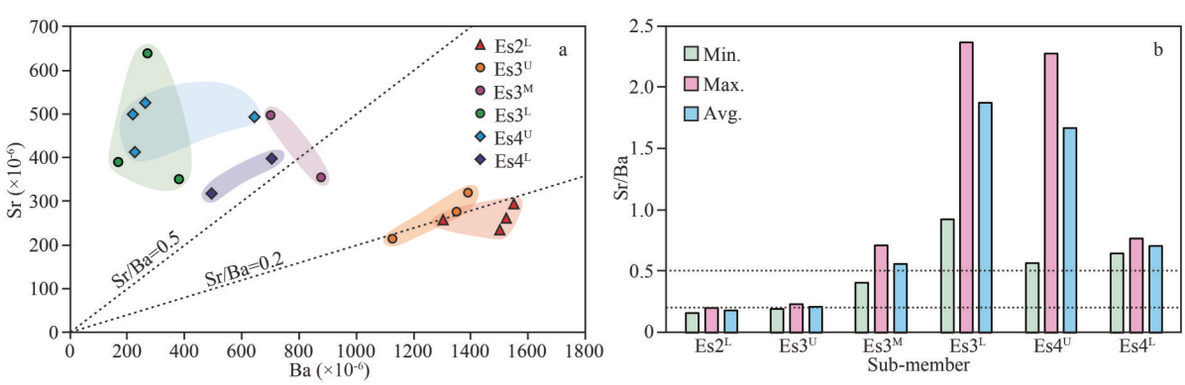

Fig.5 Sr versus Ba cross-plots (a) and Sr/Ba histograms (b) in the study interval

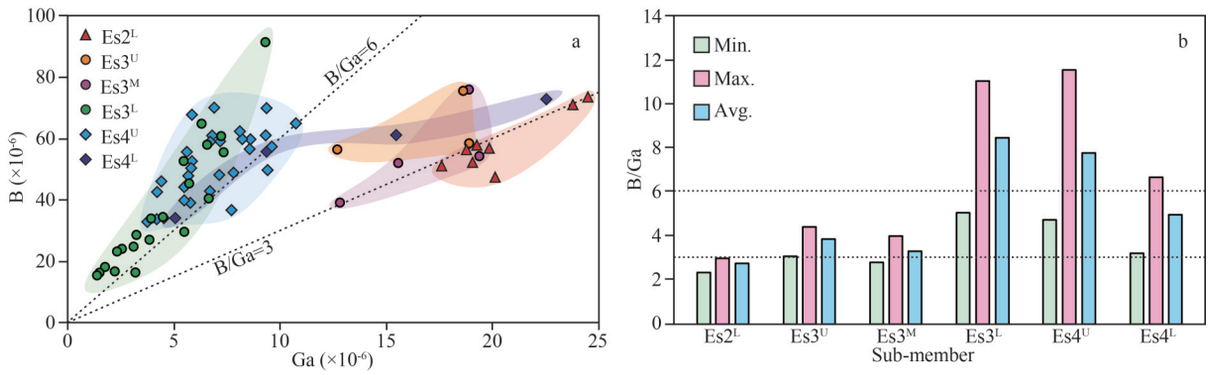

Fig.6 B versus Ga cross-plots (a) and B/Ga histograms (b) in the study interval

Table 1 Relative content (%) of X-ray diffraction clay minerals in the study area

Well name	Depth (m)	Sub-member	I/S (%)	I (%)	K (%)	Ch (%)	Proportion of S in I/S (%)
Y139	2 055.83	$Es2^{L}$	63	17	13	7	40
Y139	2 058.37	$Es2^{L}$	67	15	10	8	45
Y139	2 060.23	$Es2^{L}$	63	21	12	5	40
Y139	2 063.15	$Es2^{L}$	50	27	11	12	40
Y139	2 066.28	$Es2^{L}$	60	15	15	10	40
Y139	2 070.99	$Es2^{L}$	64	9	12	15	50
Y139	2 072.96	$Es2^{L}$	72	5	9	14	50
Y139	2 075.73	$Es2^{L}$	74	9	12	5	50
YD341	3 035.40	$Es3^{U}$	64	24	10	2	45
YD341	3 038.80	$Es3^{U}$	77	22	0	1	45
YD341	3 040.90	$Es3^{U}$	76	9	12	4	45
Y171	3 031.25	$Es3^{M}$	73	13	12	2	45
Y171	3 033.80	$Es3^{M}$	48	35	13	4	50
Y171	3 034.50	$Es3^{M}$	60	23	12	5	50
Y171	3 035.21	$Es3^{M}$	74	11	10	5	50
L67	3 243.83	$Es3^{L}$	76	18	2	4	25
L67	3 245.41	$Es3^{L}$	49	16	20	15	25
L67	3 246.42	$Es3^{L}$	50	41	4	5	25
L67	3 272.75	$Es3^{L}$	72	24	4	0	25
L67	3 275.76	$Es3^{L}$	69	21	6	4	40
L67	3 299.73	$Es3^{L}$	75	20	5	0	40
L67	3 300.73	$Es3^{L}$	70	24	6	0	40
L67	3 303.15	$Es3^{L}$	90	10	0	0	40
L67	3 305.80	$Es3^{L}$	78	12	5	5	50
L67	3 306.20	$Es3^{L}$	73	27	0	0	40
L67	3 307.14	$Es3^{L}$	67	23	5	5	20
L67	3 309.07	$Es3^{L}$	76	14	10	0	25
L67	3 309.14	$Es3^{L}$	65	15	10	10	40
L67	3 310.01	$Es3^{L}$	74	21	0	5	35
L67	3 310.50	$Es3^{L}$	68	32	0	0	50
L67	3 312.59	$Es3^{L}$	79	16	3	2	60
L67	3 318.57	$Es3^{L}$	76	15	1	8	60
L67	3 340.90	$Es3^{L}$	60	16	19	5	35
L67	3 342.45	$Es3^{L}$	54	20	19	7	40

To be continued

Table 1 Continued

Well name	Depth (m)	Sub-member	I/S (%)	I (%)	K (%)	Ch (%)	Proportion of S in I/S (%)
L67	3 344.85	$Es3^{L}$	56	23	16	5	30
L67	3 346.75	$Es3^{L}$	54	30	10	6	20
L22	1 660.85	$Es4^{U}$	53	22	11	15	40
L22	1 661.55	$Es4^{U}$	60	27	6	7	20
L22	1 662.01	$Es4^{U}$	56	32	6	6	55
L22	1 662.32	$Es4^{U}$	53	17	15	15	55
L22	1 663.90	$Es4^{U}$	69	11	18	2	55
L22	1 666.00	$Es4^{U}$	51	35	11	3	55
L22	1 668.00	$Es4^{U}$	60	14	12	14	55
L22	1 669.20	$Es4^{U}$	67	14	12	7	55
L22	1 672.30	$Es4^{U}$	62	18	6	14	55
L22	1 676.84	$Es4^{U}$	45	45	5	5	45
L22	1 682.60	$Es4^{U}$	59	20	9	11	45
L22	1 688.00	$Es4^{U}$	37	35	13	15	45
L22	1 695.45	$Es4^{U}$	60	16	12	12	55
L22	1 701.00	$Es4^{U}$	60	19	9	12	55
L22	1 708.70	$Es4^{U}$	71	8	12	9	55
L22	1 711.70	$Es4^{U}$	46	32	8	14	50
L22	1 713.77	$Es4^{U}$	54	18	13	15	50
L22	1 719.70	$Es4^{U}$	42	24	19	15	25
L22	1 729.80	$Es4^{U}$	68	22	7	3	50
L22	1 734.50	$Es4^{U}$	76	6	11	7	50
L22	1 748.10	$Es4^{U}$	80	11	6	3	40
L22	1 750.85	$Es4^{U}$	77	15	5	3	40
L22	1 760.55	$Es4^{U}$	60	16	9	15	50
L22	1 762.01	$Es4^{U}$	78	13	5	4	40
L22	1 763.32	$Es4^{U}$	83	12	5	0	40
L22	1 764.90	$Es4^{U}$	70	25	5	0	40
L22	1 766.00	$Es4^{U}$	77	19	5	0	50
L22	1 767.00	$Es4^{U}$	73	21	5	0	50
L22	1 769.20	$Es4^{U}$	73	22	5	0	30
L22	1 771.30	$Es4^{U}$	73	23	2	2	30
L22	1 773.50	$Es4^{U}$	83	7	10	0	30
SG4	2 969.30	$Es4^{L}$	58	16	11	15	50
SG4	2 971.50	$Es4^{L}$	67	4	11	18	60
SG4	2 973.40	$Es4^{L}$	61	19	15	5	50
SG4	2 973.50	$Es4^{L}$	58	15	17	10	50

I/S: illite/smectite mixed layer, I: illite, K: kaolinite, Ch: chlorite, S: smectite.

Our results indicate that the highest paleosalinity value from Couch's method in the study area was 11.9, the lowest was 3.1 and the mean value was 7.4. We also gathered statistics for the maximum, minimum and mean values of S_{pc} in different sub-members (Fig.7a). Furthermore, we constructed a frequency distribution histogram of the number of S_{pc} occurrences in the Middle-Late Eocene water body (Fig.7b), with the highest frequency of S_{pc} ranging from 7 to 9, primarily in $Es3^{L}$ and $Es4^{U}$, and sporadic occurrences in $Es3^{M}$ and $Es4^{L}$. The lower frequency of S_{pc} was concentrated in $Es2^{L}$, $Es3^{U}$, $Es3^{M}$, and $Es4^{U}$.

5 DISCUSSION

5.1 Provenance and diagenesis

The provenance and its variations can have an impact on the indicators of geochemical elements, leading to potential uncertainties in paleosalinity reconstruction (Sun et al., 2022b). Previous research indicated that the sediment provenance of the Eocene Shahejie Formation in the Zhanhua Sag originates from the Chengdong Uplift, Chenjiazhuang Uplift, and Yihezhuang Uplift (Liu et al., 2016). However, due to the consistent sedimentary background in the basin, the provenance components

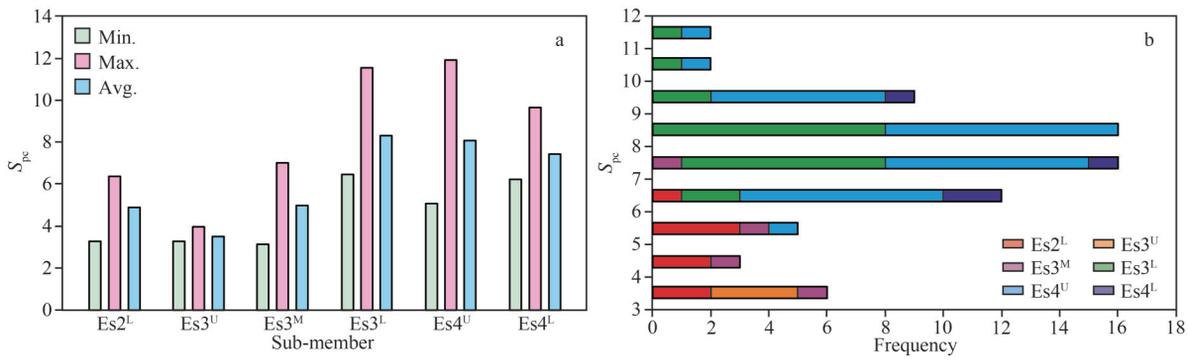

Fig.7 Histograms of minimum, maximum, and average values of S_{pc} (a) for each sub-member, and those of the frequency distribution of S_{pc} (b) for each sub-member

of these three uplifts are similar enough (Liu et al., 2020b) that any changes in elemental geochemical indicators caused by variations in provenance components can be disregarded. Nonetheless, it is important to consider that the nature of the provenance itself can also influence paleosalinity indicators. For example, clay minerals contain B, which can arise from both adsorption during sedimentation and the weathering of granite amphibolite to form illite. Previous studies have demonstrated that the inherited B content of illite is largely proportional to its illite content (Ye et al., 2016), necessitating the elimination of inherited B. The study interval exhibits relatively low potassium feldspar content, with only 3 out of 71 samples containing potassium feldspar, and their content does not exceed 5% of the whole rock composition. Therefore, any paleosalinity errors resulting from the presence of inherited B can be disregarded. Additionally, Ga is predominantly present in clay minerals and does not undergo significant absorption from seawater. Consequently, the B/Ga ratio remains unaffected as Ga implicitly normalizes for variation in host-rock lithology.

Although diagenesis is known to have minimal impact on the abundance of Sr, Ba, B, and Ga in clay minerals (Ye et al., 2016; Wei and Algeo, 2020), it can still affect the relative proportion of clay minerals and thus impact the estimation of B content adsorbed by clay minerals. Previous research demonstrated that the most common transformation during burial is the conversion of smectite into illite (Chamley, 1994). This transformation is significant for paleosalinity reconstructions due to the strong B adsorption capacity of illite (Walker and Price, 1963; Walker, 1968). The classic diagenetic model suggests that the content and proportion of illite in I/S increase gradually with depth (Weaver, 1984). However, among the 71 samples examined in this study interval, the relatively stable proportion of illite in I/S indicates a limited and uniform intensity of diagenesis, suggesting negligible changes in diagenesis.

5.2 Discrimination of water body types

The Sr/Ba ratio is a semi-quantitative proxy for the salinity reconstruction of paleowater body and has been applied sporadically to lacustrine systems and marginal marine environments (Chen et al., 1997, 2000). Unlike Ba, Sr has a higher solubility and migrates more readily in solution. As the salinity of the water body increases, Ba precipitates first as $BaSO_4$, while Sr requires higher salinity to precipitate as $SrSO_4$ (Zhang et al., 2017). Thus, $BaSO_4$ is mainly deposited in shallow waters and the marine-continental transitional zone, whereas $SrSO_4$ is deposited in deep-sea sediments (Wang et al., 1979). Therefore, the Sr/Ba ratio can accurately characterise the water body salinity and its media properties. Previous studies have shown that the Sr/Ba ratio of terrestrial fresh water is less than 0.2, brackish water ranges from 0.2 to 0.5 and salty water is generally higher than 0.5 (Wei and Algeo, 2020). The Sr/Ba ratios of Es3^{M}, Es3^{L}, Es4^{U}, and Es4^{L} all indicate characteristics different from fresh water, as shown by the distribution intervals of salinity proxies for all samples (Fig.5a) and the mean values for each sub-member (Figs.5b & 8a). Although all four sub-members indicate a saline environment, the salinity of water body during the depositional period of Es3^{M} and Es4^{L} is significantly lower than the other two sub-members. Furthermore, as sedimentation progressed in the basin, the Sr/Ba ratios in Es3^{U} and Es3^{M} typically fall within the range of 0.2 to 0.7, showing a brackish character

with a mixture of salty and fresh water, especially in $Es3^{M}$, which exhibits a transitional type with a maximum value close to brackish water and a minimum value of fresh water. Up to $Es2^{L}$, the Sr/Ba ratio proxy exhibits the total freshwater characteristics of the environment (Fig.8a), which may indicate a trans-humidification of the closed lake basin climate or a marine regression event in the open basin.

The B/Ga ratio is a reliable indicator of paleosalinity recovery in deep-time mud shale formations. This is because B and Ga are both B group elements in the periodic table with identical valences (+3) and similar abundances but divergent concentrations and geochemical behaviours in fresh water and marine systems (Liu et al., 2020a; Wei et al., 2022). Investigations of modern and ancient aqueous systems have confirmed a strong positive relationship between water body salinity types and B and Ga contents. B/Ga ratio ranges of <3, 3–6, and >6 are associated with mudstones and shales from fresh water, brackish water and salty water, respectively (Wei and Algeo, 2020). In the study area, most samples recorded salty water conditions from $Es4^{U}$ to $Es3^{L}$ (mean >6), brackish salinity from $Es3^{M}$ to the $Es3^{U}$ (mean ~4) and a freshwater environment in $Es2^{L}$ (mean <3). These salinity conditions were determined using predetermined thresholds for B/Ga ratios, indicating a generally reduced salinity condition (Figs.6b & 8b).

According to the salinity value, the types of water body are divided into fresh water (<0.5), brackish water (0.5–30) and salty water (>30). Brackish water can be further divided into three subtypes: oligohaline (0.5–5), mesohaline (5–18), and polyhaline (>18) (Zhang et al., 2017). In the Middle-Late Eocene of the Zhanhua Sag, the paleosalinity values using Couch's paleosalimeter were determined to be in the brackish water range. A detailed analysis demonstrates that the paleosalinity values obtained using Couch's method were divided into mesohaline brackish water from $Es4^{L}$ to $Es3^{L}$ and oligohaline brackish water from $Es3^{M}$ to $Es2^{L}$ (Fig.8c).

5.3 Evaluation of paleosalinity proxies

The three paleosalinity proxies mentioned above indicate a high degree of consistency in paleosalinity variation during the Middle-Late Eocene (Figs.8–9). Notably, the Sr/Ba and B/Ga ratios demonstrate greater sensitivity in reflecting the significant increase in salinity from $Es4^{L}$ to $Es4^{U}$. However, further evaluation is necessary to confirm the presence of this event and validate the credibility of the proxies. Previous paleosalinity studies in the region have reported an increase in salinity during this period (Li and Xiao, 1988; Zhang et al., 2020), supporting the reliability of the elemental ratio proxies in this study. Of all the paleosalinity proxies

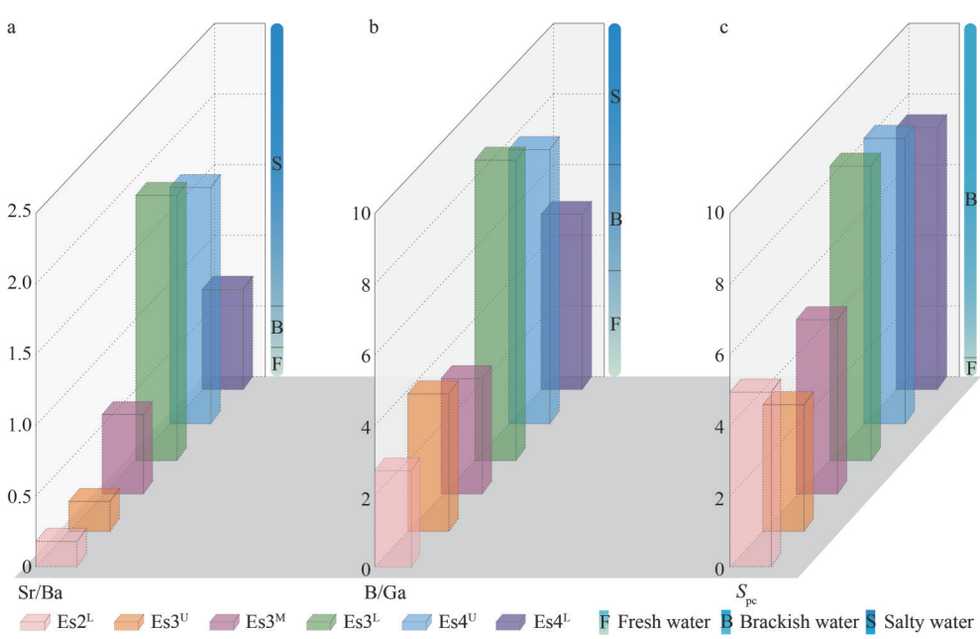

Fig.8 The distribution of mean paleosalinity proxies for each sub-member in the Middle-Upper Eocene Shahejie Formation of the Zhanhua Sag

a. Sr/Ba; b. B/Ga; c. S_{pc}.

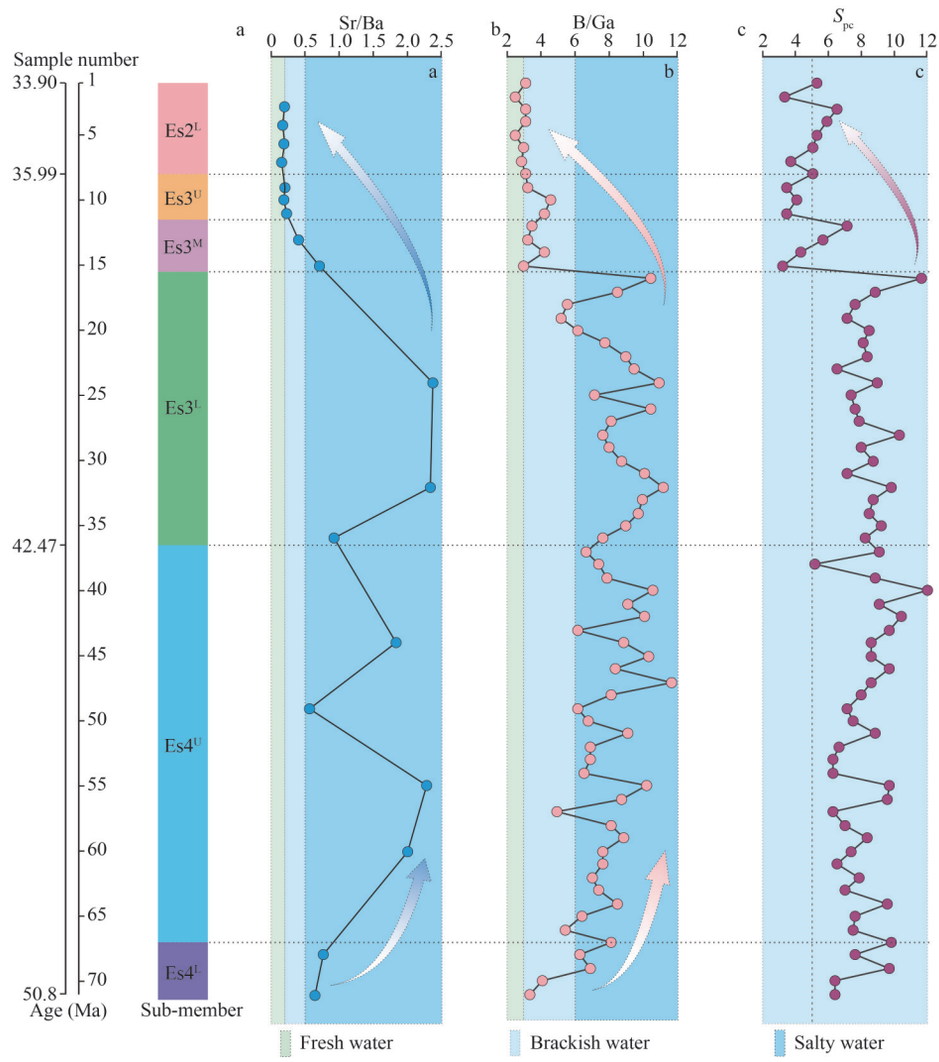

Fig.9 Evolutionary profiles of multiple paleosalinity proxies of Middle-Upper Eocene Shahejie Formation in the Zhanhua Sag

a. Sr/Ba; b. B/Ga; c. S_{pc}. All samples are not from the same well but follow the up-and-down sequence of stratigraphic comparisons. The order in the profiles represents the relative time sequence but not the absolute geological age. The horizontal dotted lines are the boundaries of the sub-members, and the vertical dotted lines are the thresholds of the paleosalinity types.

discussed above, Couch's salinometer is generally considered the most accurate by sedimentologists as it accounts for the variability in B sorption by different clay minerals (Ye et al., 2016; Zhang et al., 2017). While Couch's salinometer is capable of quantifying salinity values, it is susceptible to diagenesis disturbances. When Sr/Ba ratio is applied, it is necessary to eliminate the carbonate-sourced Sr, which will result in the deletion of carbonate-containing sample points and reduce the resolution of paleosalinity prediction. In contrast, the B/Ga ratio is often more sensitive to changes in salinity and has higher resolution. This method can implicitly normalize for variation in host-rock lithology.

The evolutionary profiles of paleosalinity proxies revealed that the B/Ga ratio is the most significant parameter for distinguishing the salinity types of water body in the study area (Fig.9). From the evolutionary profile, it becomes evident that the B/Ga ratio provides enhanced resolution for paleosalinity prediction compared to the Sr/Ba ratio, as it allows for a greater number of samples to be analyzed within the same layer thickness. Moreover, the B/Ga ratio exhibits higher sensitivity to the salinity range of water bodies compared to Couch's paleosalinity meter. This is particularly evident in the accurate prediction of fresh water in $Es2^L$ using the B/Ga ratio. However, it should be noted that the range of variation in Couch's paleosalinity meter is relatively limited, as all samples fall within the brackish water category. The reconstruction outcomes

represent the paleosalinity types of the study intervals, indicating the existence of three paleosalinity types, namely fresh water ($Es2^{L}$), brackish water ($Es3^{U}$, $Es3^{M}$, and $Es4^{L}$) and salty water ($Es3^{L}$ and $Es4^{U}$). there was a single salinity transition from marine to low-brackish or freshwater at around 40–38 Ma. It is of considerable significance to highlight that, at the turn of the $Es3^{L}$ and $Es3^{M}$ sedimentary periods, an unmistakable salinity transition occurs. This transition involves a noteworthy shift from salty water to low-brackish or freshwater conditions. Its occurrence potentially signifies notable changes in the driving forces that influence salinity within the specific context of East Asia, including factors like eustatic sea level changes, climatic fluctuations, and the ongoing tectonic evolution of the region.

5.4 Paleoclimatic and eustatic implication

The primary factor controlling the salinity of watermasses in terrestrial lakes is whether the lake basin is closed. In closed lake basins, the balance of regional precipitation and evaporation typically determines the salinity of lake water. Therefore, it is considered a sensitive proxy for the climate in arid and semi-arid regions (Ye et al., 2016). Under stable tectonic conditions, high-salinity lake water is mostly associated with low precipitation or high evaporation under arid climatic conditions, whereas low-salinity lake water is often associated with high precipitation and low evaporation produced by a relatively wet climate. Therefore, climatic conditions significantly influence the salinity of watermasses in closed lake basins, which is mostly associated with the global climatic context and regional topographic rainfall generated by tectonic movements. Conversely, the salinity of watermasses in open offshore lake basins fluctuates due to frequent marine intrusion. Using seawater promotes the stratification of the water column and increases the salinity difference in the vertical direction of the watermass (Erbacher et al., 2001; Wei et al., 2018). Following marine intrusion, the effects of regional precipitation and evaporation on salinity become weak to negligible at higher lake levels.

The influence of climatic factors on the salinity of closed watermasses in the Middle Eocene should not be underestimated. Evidence from both terrestrial fossils and elemental geochemical characteristics suggests the presence of a closed lacustrine facies prior to the upper sub-member of the 4th member (Li and Xiao, 1988; Yao and Millero, 1996; Wang et al., 2015; Wei et al., 2018). Conversely, stable, and continuous red beds, evaporites, sporopollenin fossils of *Ephedra* and a high paleoclimatic index indicate relatively arid climatic conditions (Fig.10) in the lower sub-member of the 4th member of the Shahejie Formation (Walker, 1967, 1974; Cao et al., 2011; Chen et al., 2021). In addition to the influence of global climate change, the reduction in regional precipitation and the increase in evapotranspiration have created favourable conditions for the formation of an arid climate.

Paleogeographic reconstructions suggest that the Bohai Bay Basin was intermittently connected to the seawater of the Pacific Ocean since the Cretaceous Period (Hou et al., 2000; Wei et al., 2021). Therefore, it is inadequate to establish the mechanisms causing paleosalinity variation solely from the perspective of paleoclimatic evolution. Although extensive evidence of marine transgression in paleontology, facies minerals, and elemental geochemistry has been reported (He and Yu, 1982; Li and Xiao, 1988), the period and location of marine transgression events remain highly debated. The most probable location is the northeastern margin of the basin, which is bound by the Tanlu Fault Zone (Cao et al., 2015).

The marine fossils indicate marine transgression events during the depositional period of $Es4^{U}$ and $Es3^{L}$ (Fig.10). The tectonic low sill between the Liaodong Uplift and the Jiaodong Uplift is a low-lying zone where the Eocene Bohai Bay lacustrine system is interconnected with the Pacific Ocean (Wang et al., 2015; Zhao et al., 2018). Consequently, the pre-existing terrestrial lacustrine system was linked to the ocean whenever the global sea level rose by several tens of metres (Wei et al., 2021). Reports of global sea level rise (Haq et al., 1987; Miller et al., 2005) support our hypothesis. As mentioned in the introduction, the model developed by Wei et al. (2018) established a mechanism of marine transgression on salinity, without discussing the significance of coupled climatic and eustatic evolutionary mechanisms on the salinity variation of the Middle-Late Eocene watermasses.

Our study postulated that the salinity of the watermass in the Zhanhua Sag undergoes a transition from freshwater to brackish water during the depositional period of $Es4^{L}$ (after ~50.8 Ma). This change in salinity is likely due to the arid climate in the basin, leading to the gradual drying up of salt lakes and increased evaporation compared to

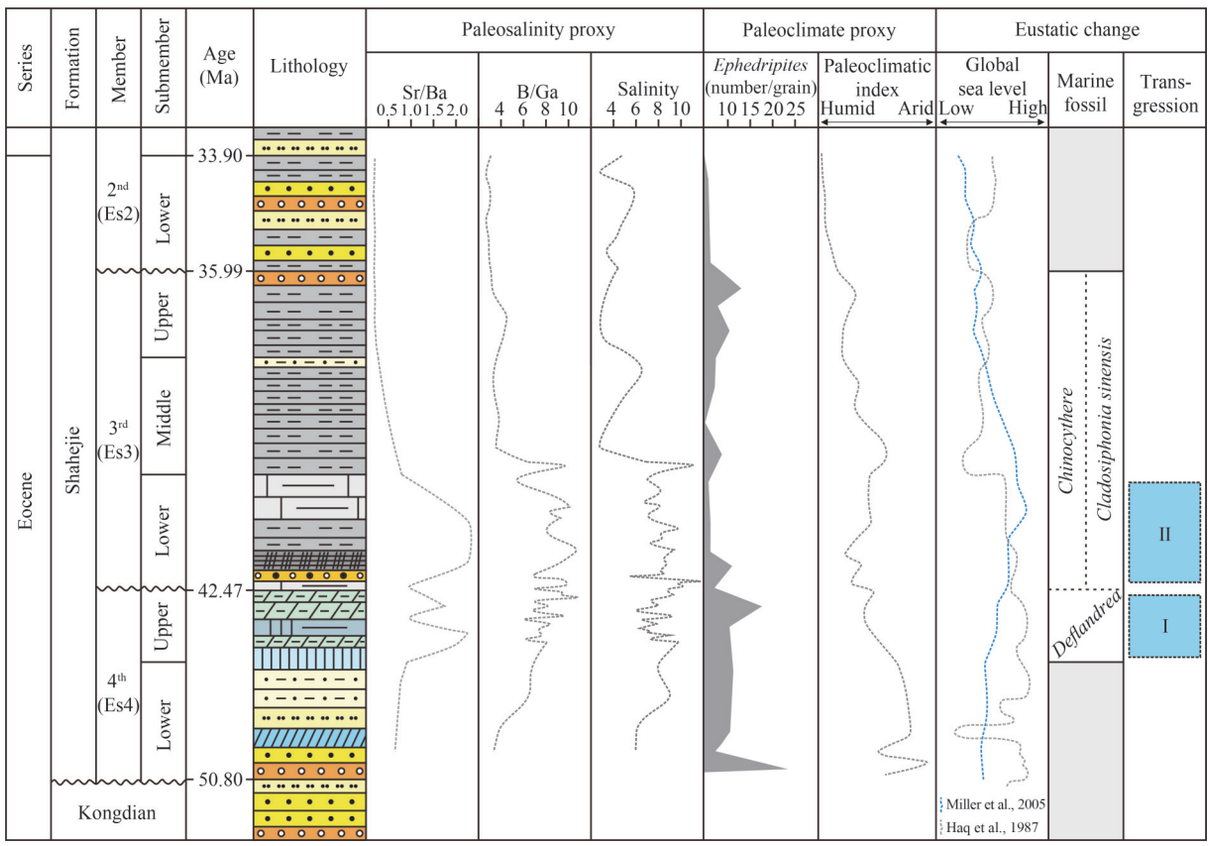

Fig.10 Paleoenvironmental evolution profile of the Eocene in the Bohai Bay Basin

Ages are based on the astronomical timescale of Liu et al. (2018); paleosalinity proxies are based on this study; paleoclimate proxies are based on Chen et al. (2021); global sea level curves are from Haq et al. (1987) (grey dashed) and Miller et al. (2005) (blue dashed); marine fossil and marine transgression events are from Yuan et al. (2005) and Wei et al. (2018).

precipitation (Fig.11a). The disruption of the lake basin by frequent marine incursion events (Wei et al., 2018) during the depositional period of $Es4^{U}$ (before ~42.47 Ma), caused by global sea level rise (Haq et al., 1987; Miller et al., 2005), provides an explanation for the unusually high salinity values (Fig.10). Until the depositional period of $Es3^{L}$ (after ~42.47 Ma), large-scale marine transgression replaced intermittent marine incursion events, introducing seawater, and maintaining the presence of salt in the lake basin. Notably, the seawater injected into the lake basin provided a brine source for evaporites and reduced the drought threshold of the climate for the formation of gypsum rocks. The climate during this period was semi-arid and more humid than $Es4^{L}$ (Fig.10). Thus, marine transgression events should be considered as the primary factor controlling the high salinity of salty water in $Es4^{U}$ and $Es3^{L}$, rather than climate. The rise in sea level effectively fuelled the salinity surge and injected marine ecology into the original terrestrial lake basin (Fig.11b). Subsequently, the continued decline in global sea level marked the end of the marine transgression. While intermittent sea level rises can sporadically trigger transgressive events and contribute to the presence of salts, the salinity of the lake is primarily influenced by semi-arid climate, leading to the formation of brackish water (Fig.11c). Until the sea level drops far below the marginal sill, the lake was completely isolated from the ocean, presenting an independent lake ecology and watermass salinity pattern. At this stage, the humid climate encourages the salinity of the watermasses to transform into freshwater (Fig.11d).

The climatic and eustatic mechanisms model can provide a systematic theoretical pattern for paleosalinity variation in all offshore basins. It is evident that regional climate evolution is an important causal factor in the basin salinity variation when the offshore basin is completely unaffected by marine incursions (patterns presented in Fig.11a–d). This paper focuses on regional climate change and its influence on watermass salinity through the equilibrium relationship between evaporation and

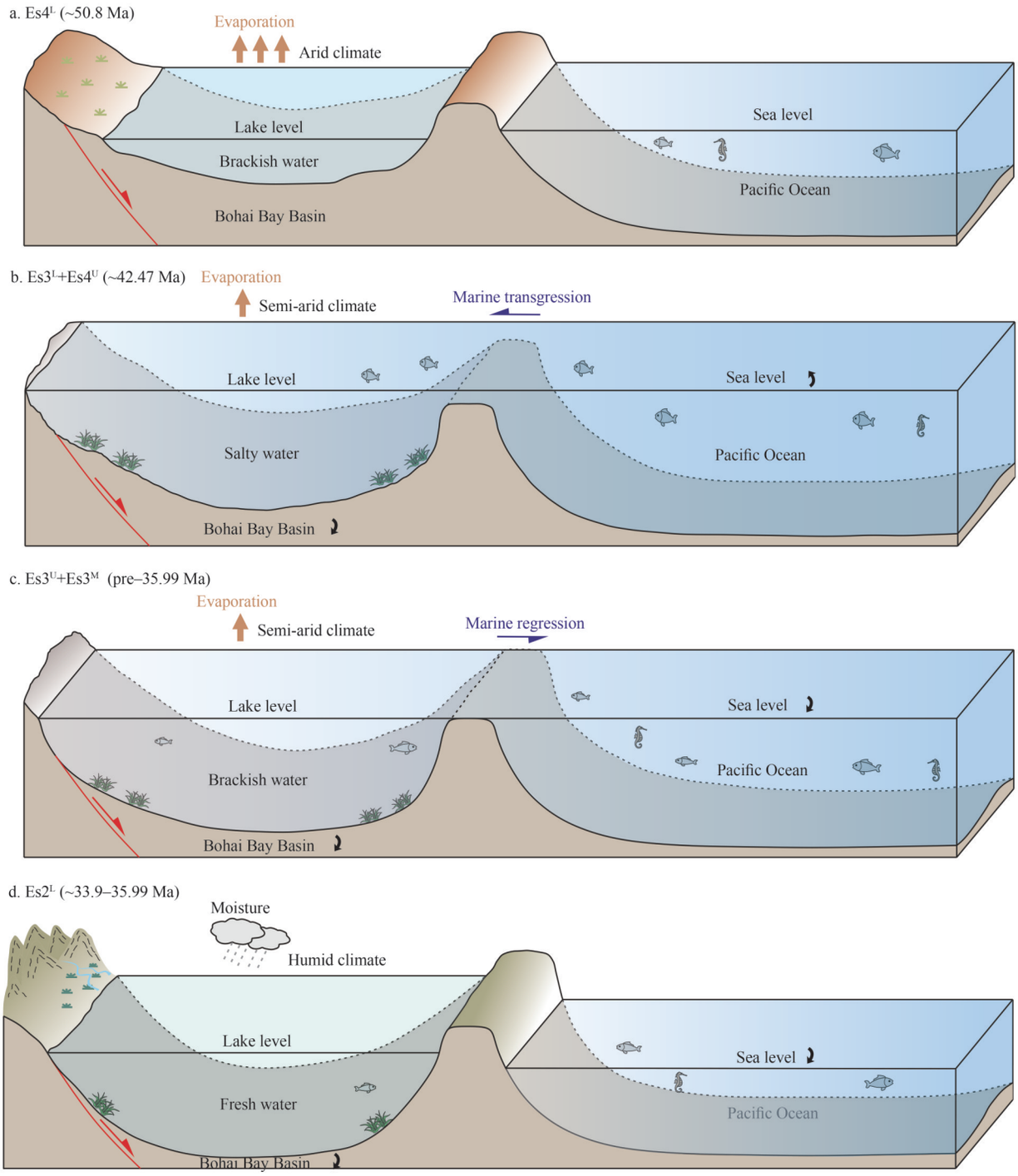

Fig.11 Models of climatic and eustatic mechanisms for paleosalinity variation during the Eocene Shahejie Formation in Zhanhua Sag

The black arrow represents the ascending and descending directions, (a), (c), and (d) are mainly affected by climate, (b) is mainly controlled by eustasy.

precipitation. However, when the offshore basin is affected by marine transgression, the salinity of the watermass fluctuates due to the injection and withdrawal of seawater. Notably, variations in paleoclimate and eustasy often occur simultaneously. Therefore, it is necessary to extensively explore the main driving forces affecting the salinity variation when applying this model.

6 CONCLUSION

The paleosalinity in the Middle-Upper Eocene Shahejie Formation in the Zhanhua Sag was reconstructed using multiple-element geochemistry proxies. The findings reveal the characteristics of paleosalinity variation in the study area. The conclusions of this study are as follows.

The Sr/Ba, B/Ga, and Couch's paleosalimeter can effectively differentiate between water body with varying paleosalinity. Sr/Ba and B/Ga ratios indicate salty water deposition from $Es4^{L}$ to $Es3^{L}$, brackish water deposition during $Es3^{M}$ and $Es3^{U}$ and freshwater deposition during $Es2^{L}$. The salinity values of Couch's method ranges from 3.1 to 11.9, reflecting the overall characteristics of oligohaline to mesohaline brackish water.

We investigated the temporal variation in paleosalinity during the Middle-Upper Eocene Shahejie Formation in the Zhanhua Sag, Jiyang Depression, Bohai Bay Basin. All three paleosalinity proxies showed very similar variation trends, specifically the Sr/Ba and B/Ga ratios, after eliminating the effects of carbonate-sourced Sr. These ratios exhibited a clear upward and then downward trend from the deposition periods of $Es4^{L}$ to $Es2^{L}$. Among the five paleosalinity proxies, the B/Ga ratio had the highest reliability and resolution in determining the salinity types of water body in the study area. The threshold value-based result reflected three paleosalinity types of water body in the study interval: brackish water, salty water, and fresh water.

In the paleoenvironmental reconstruction of offshore lacustrine basins, it is essential to determine the main environmental driving forces through a comprehensive analysis of salinity, climate and eustasy. Unlike closed lacustrine basins, the paleosalinity variation of offshore lacustrine basins is not solely controlled by regional drought and humidity but also depends on the coupling effect of regional climate and eustasy. Therefore, only considering changes in regional climate cannot accurately explain the salinity variation of all offshore lacustrine basins at any time. For example, the joint action of sea level rise and regional climate drought can exacerbate the surge of salinity, and an increase in water salinity can also occur under humid climate conditions during the marine transgression period. Therefore, changes in climate and eustasy alone cannot indicate paleosalinity variation. Conversely, only the paleosalinity variation of offshore lacustrine basins cannot be used to indicate paleoclimatic change.

7 DATA AVAILABILITY STATEMENT

The data that support the findings of this study are available from the corresponding author upon reasonable request.

8 ACKNOWLEDGMENT

We thank SINOPEC Exploration and Production Research Institute of Shengli Oilfield for providing valuable opportunities for core observation and description, sampling, and element geochemical data. We are grateful to Professor Thomas J. ALGEO and other reviewers for their constructive comments, which have greatly improved the quality of this paper.

References

Adams T D, Haynes J R, Walker C T. 1965. Boron in Holocene illites of the Dovey Estuary, Wales, and its relationship to palaeosalinity in cyclothems. *Sedimentology*, **4**(3): 189-195, https://doi.org/10.1111/j.1365-3091.1965.tb01288.x.

Cai G Q, Guo F, Liu X T et al. 2011. Elemental and Sr-Nd isotopic compositions of Cenozoic sedimentary rocks from the Dongying Sag of Jiyang Depression, North China: implications for provenance evolution. *Geochemical Journal*, **45**(1): 33-55, https://doi.org/10.2343/geochemj.1.0092.

Cao X Z, Li S Z, Xu L Q et al. 2015. Mesozoic-Cenozoic evolution and mechanism of tectonic geomorphology in the central North China Block: constraint from apatite fission track thermochronology. *Journal of Asian Earth Sciences*, **114**: 41-53, https://doi.org/10.1016/j.jseaes.2015.03.041.

Cao Y C, Wang J, Gao Y J et al. 2011. Sedimentary characteristics and model of red beds-gypsum salt beds of the Paleogene in Dongying Sag, Jiyang Depression. *Journal of Palaeogeography*, **13**(4): 375-386. (in Chinese with English abstract)

Chamley H. 1994. Clay mineral diagenesis. *In*: Parker A, Sellwood B W eds. Quantitative Diagenesis: Recent Developments and Applications to Reservoir Geology. Springer, Dordrecht. p.161-188, https://doi.org/10.1007/978-94-011-0189-9_5.

Chen T, Zhang J L, Li Y et al. 2021. Quantitative reconstruction of the palaeoclimate of the Shahejie Formation in the Chezhen Depression, Bohai Bay Basin, eastern China. *Frontiers of Earth Science*, **15**(4): 909-921, https://doi.org/10.1007/s11707-021-0932-7.

Chen Z Y, Chen Z L, Zhang W G. 1997. Quaternary stratigraphy and trace-element indices of the Yangtze Delta, Eastern China, with special reference to marine transgressions. *Quaternary Research*, **47**(2): 181-191, https://doi.org/10.1006/qres.1996.1878.

Chen Z Y, Song B P, Wang Z H et al. 2000. Late Quaternary

evolution of the sub-aqueous Yangtze Delta, China: sedimentation, stratigraphy, palynology, and deformation. *Marine Geology*, **162**(2-4): 423-441, https://doi.org/10.1016/S0025-3227(99)00064-X.

Couch E L. 1971. Calculation of paleosalinities from boron and clay mineral data. *AAPG Bulletin*, **55**(10): 1829-1837, https://doi.org/10.1306/819A3DAC-16C5-11D7-8645000102C1865D.

Degens E T, Williams E G, Keith M L. 1957. Environmental studies of carboniferous sediments. Part I: geochemical criteria for differentiating marine from fresh-water shales. *AAPG Bulletin*, **41**(11): 2427-2455, https://doi.org/10.1306/0BDA59A5-16BD-11D7-8645000102C1865D.

Edgell H S. 1996. Salt tectonism in the Persian Gulf basin. *Geological Society*, *London*, *Special Publications*, **100**(1): 129-151, https://doi.org/10.1144/gsl.sp.1996.100.01.10.

Erbacher J, Huber B T, Norris R D et al. 2001. Increased thermohaline stratification as a possible cause for an ocean anoxic event in the Cretaceous period. *Nature*, **409**(6818): 325-327, https://doi.org/10.1038/35053041.

Haq B U, Hardenbol J, Vail P R. 1987. Chronology of fluctuating sea levels since the Triassic. *Science*, **235**(4793): 1156-1167, https://doi.org/10.1126/science.235.4793.1156.

Harder H. 1970. Boron content of sediments as a tool in facies analysis. *Sedimentary Geology*, **4**(1-2): 153-175, https://doi.org/10.1016/0037-0738(70)90009-6.

He J Y, Yu S Y. 1982. Occurrence of glauconite in lower tertiary of northern Huang-Hua Depression. *Earth Science*, (1): 129-143. (in Chinese with English abstract)

Hou D J, Li M W, Huang Q H. 2000. Marine transgressional events in the gigantic freshwater lake Songliao: paleontological and geochemical evidence. *Organic Geochemistry*, **31**(7-8): 763-768, https://doi.org/10.1016/S0146-6380(00)00065-6.

Hua Y Q, Guo X W, Tao Z et al. 2021. Mechanisms for overpressure generation in the Bonan sag of Zhanhua depression, Bohai Bay Basin, China. *Marine and Petroleum Geology*, **128**: 105032, https://doi.org/10.1016/j.marpetgeo.2021.105032.

Hudec M R, Jackson M P A. 2006. Advance of allochthonous salt sheets in passive margins and orogens. *AAPG Bulletin*, **90**(10): 1535-1564, https://doi.org/10.1306/05080605143.

Jiang F J, Chen D, Zhu C X et al. 2022. Mechanisms for the anisotropic enrichment of organic matter in saline lake basin: a case study of the Early Eocene Dongpu Depression, eastern China. *Journal of Petroleum Science and Engineering*, **210**: 110035, https://doi.org/10.1016/J.PETROL.2021.110035.

Li C F, Xiao J F. 1988. The application of trace element to the study on paleosalinities in Shahejie Formation of Dongying Basin Shengli oilfield. *Acta Sedimentologica Sinica*, **6**(4): 100-107. (in Chinese with English abstract)

Li T W, Jiang Z X, Xu C L et al. 2017. Effect of pore structure on shale oil accumulation in the lower third member of the Shahejie formation, Zhanhua Sag, eastern China: evidence from gas adsorption and nuclear magnetic resonance. *Marine and Petroleum Geology*, **88**: 932-949, https://doi.org/10.1016/j.marpetgeo.2017.09.030.

Li Y, Zhang J L, Xu Y H et al. 2022. Genetic mechanism and grading assessment of the glutenite reservoirs in the Eocene Shahejie Formation, Chezhen Sag, Bohai Bay Basin. *Journal of Petroleum Science and Engineering*, **211**: 110226, https://doi.org/10.1016/j.petrol.2022.110226.

Li Y Y, Zha M, Song R C et al. 2021. Microstructure and pore systems of shallow-buried fluvial mudstone caprocks in Zhanhua depression, East China inferred from SEM and MICP. *Marine and Petroleum Geology*, **132**: 105189, https://doi.org/10.1016/j.marpetgeo.2021.105189.

Liu B, Song Y, Zhu K et al. 2020a. Mineralogy and element geochemistry of salinized lacustrine organic-rich shale in the middle Permian Santanghu Basin: implications for paleoenvironment, provenance, tectonic setting and shale oil potential. *Marine and Petroleum Geology*, **120**: 104569, https://doi.org/10.1016/j.marpetgeo.2020.104569.

Liu L, Chen H D, Wen H G et al. 2020b. Facies architecture and sediment infilling processes in intrabasinal slope belts of lacustrine rift basins, Zhanhua Depression, Bohai Bay Basin. *Marine and Petroleum Geology*, **112**: 104089, https://doi.org/10.1016/j.marpetgeo.2019.104089.

Liu L, Wen H G, Chen H D et al. 2021. Depositional architectures and evolutional processes of channel systems in lacustrine rift basins: the Eocene Shahejie Formation, Zhanhua depression, Bohai Bay Basin. *Marine and Petroleum Geology*, **131**: 105155, https://doi.org/10.1016/j.marpetgeo.2021.105155.

Liu Q H, Zhu X M, Yang Y et al. 2016. Sequence stratigraphy and seismic geomorphology application of facies architecture and sediment-dispersal patterns analysis in the third member of Eocene Shahejie Formation, slope system of Zhanhua Sag, Bohai Bay Basin, China. *Marine and Petroleum Geology*, **78**: 766-784, https://doi.org/10.1016/j.marpetgeo.2015.11.015.

Liu Z H, Huang C J, Algeo T J et al. 2018. High-resolution astrochronological record for the Paleocene-Oligocene (**66**-23 Ma) from the rapidly subsiding Bohai Bay Basin, Chinanortheastern. *Palaeogeography*, *Palaeoclimatology*, *Palaeoecology*, **510**: 78-92, https://doi.org/10.1016/j.palaeo.2017.10.030.

Ma X, Hua A, Li J et al. 2000. Salt Oil and Gas Basin. Petroleum Industry Press, Beijing. p.1-110. (in Chinese)

Miller K G, Kominz M A, Browning J V et al. 2005. The Phanerozoic record of global sea-level change. *Science*, **310**(5752): 1293-1298, https://doi.org/10.1126/science.1116412.

National Energy Administration. 2010. SY/T 5163-2010 Analysis method for clay minerals and ordinary non-clay minerals in sedimentary rocks by the X-ray diffraction. Petroleum Industry Press, Beijing, China. (in Chinese)

Ning C X, Jiang Z X, Gao Z Y et al. 2017. Characteristics and controlling factors of reservoir space of mudstone and shale in Es3x in the Zhanhua Sag. *Marine and Petroleum Geology*, **88**: 214-224, https://doi.org/10.1016/j.

marpetgeo.2017.08.025.

Potter P E, Shimp N F, Witters J. 1963. Trace elements in marine and fresh-water argillaceous sediments. *Geochim. Cosmochim. Acta*, **27**(6): 669-694, https://doi.org/10.1016/0016-7037(63)90019-X.

Price P B, Walker R M. 1963. Fossil tracks of charged particles in mica and the age of minerals. *Journal of Geophysical Research*, **68**(16): 4847-4862, https://doi.org/10.1029/JZ068i016p04847.

Qian K, Shi H X. 1982. The choice of the method of paleosalinity determination in resources evaluation. *Petroleum Exploration and Development*, (3): 32-38. (in Chinese with English abstract)

Shi D S, Li M W, Pang X Q et al. 2005. Fault-fracture mesh petroleum plays in the Zhanhua Depression, Bohai Bay Basin: Part 2. Oil-source correlation and secondary migration mechanisms. *Organic Geochemistry*, **36**(2): 203-223, https://doi.org/10.1016/j.orggeochem.2004.09.003.

Sun L, Zhang J L, Li Y et al. 2022a. Paleosalinity and lake level fluctuations of the 3rd Member of Paleogene Shahejie Formation, Chezhen Sag, Bohai Bay Basin. *Frontiers of Earth Science*, **16**(4): 949-962, https://doi.org/10.1007/s11707-022-0979-0.

Sun L, Zhang J L, Zhang T Y et al. 2022b. Paleosalinity reconstruction for the Paleocene sequence of Lishui Sag in the East China Sea Shelf Basin. *Arabian Journal for Science and Engineering*, **47**(6): 7433-7448, https://doi.org/10.1007/s13369-022-06696-7.

Tao C Z, Yin J Y, Liu J L et al. 2015. Characteristics of hydrocarbon distribution in saline basins of the passive land margin in the South Atlantic. *Geological Review*, **61**(S1): 168-169. (in Chinese)

Walker C T. 1968. Evaluation of boron as a paleosalinity indicator and its application to offshore prospects. *AAPG Bulletin*, **52**(5): 751-766, https://doi.org/10.1306/5D25C45D-16C1-11D7-8645000102C1865D.

Walker T R. 1967. Formation of red beds in modern and ancient deserts. *GSA Bulletin*, **78**(3): 353-368, https://doi.org/10.1130/0016-7606(1967)78[353:FORBIM]2.0.CO;2.

Walker T R. 1974. Formation of red beds in moist tropical climates: a hypothesis. *GSA Bulletin*, **85**(4): 633-638, https://doi.org/10.1130/0016-7606(1974)85<633:FORBIM>2.0.CO;2.

Walker C T, Price N B. 1963. Departure curves for computing paleosalinity from boron in Illites and shale. *AAPG Bulletin*, **47**(5): 833-841, https://doi.org/10.1306/BC743A93-16BE-11D7-8645000102C1865D.

Wang F, Li J, Chen Y et al. 2015. The record of mid-Holocene maximum landward marine transgression in the west coast of Bohai Bay, China. *Marine Geology*, **359**(3): 89-95, https://doi.org/10.1016/j.margeo.2014.11.013.

Wang Y Y, Guo W Y, Zhang G D. 1979. Application of some geochemical indicators in determining of sedimentary environment of the Funing Group (Paleogene), Jinhu Depression, Kiangsu Province. *Journal of Tongji University*, (2): 51-60. (in Chinese with English abstract)

Weaver C E. 1984. Shale-Slate Metamorphism in Southern Appalachians. Elsevier, Amsterdam.

Wei W, Algeo T J. 2020. Elemental proxies for paleosalinity analysis of ancient shales and mudrocks. *Geochimica et Cosmochimica Acta*, **287**: 341-366, https://doi.org/10.1016/j.gca.2019.06.034.

Wei W, Algeo T J, Lu Y B et al. 2018. Identifying marine incursions into the Paleogene Bohai Bay Basin lake system in northeastern China. *International Journal of Coal Geology*, **200**: 1-17, https://doi.org/10.1016/j.coal.2018.10.001.

Wei W, Algeo T J, Lu Y C et al. 2021. Paleosalinity proxies and marine incursions into the paleogene Bohai Bay Basin Lake System, Northeastern China. *Acta Sedimentologica Sinica*, **39**(3): 571-592, https://doi.org/10.14027/j.issn.1000-0550.2021.004. (in Chinese with English abstract)

Wei W, Yu W C, Algeo T J et al. 2022. Boron proxies record paleosalinity variation in the North American Midcontinent Sea in response to Carboniferous glacio-eustasy. *Geology*, **50**(5): 537-541, https://doi.org/10.1130/G49521.1.

Yao W S, Millero F J. 1996. Oxidation of hydrogen sulfide by hydrous Fe(III) oxides in seawater. *Marine Chemistry*, **52**(1): 1-16, https://doi.org/10.1016/0304-4203(95)00072-0.

Ye C C, Yang Y B, Fang X M et al. 2016. Late Eocene clay boron-derived paleosalinity in the Qaidam Basin and its implications for regional tectonics and climate. *Sedimentary Geology*, **346**: 49-59, https://doi.org/10.1016/j.sedgeo.2016.10.006.

Yuan W F, Chen S Y, Zeng C M. 2005. Research development and prospects on Paleogene sea transgression in Bohai Bay Basin. *Acta Sedimentologica Sinica*, **23**(4): 604-612. (in Chinese with English abstract)

Zhang X G, Lin C Y, Zahid M A et al. 2017. Paleosalinity and water body type of Eocene Pinghu Formation, Xihu Depression, East China Sea Basin. *Journal of Petroleum Science and Engineering*, **158**: 469-478, https://doi.org/10.1016/j.petrol.2017.08.074.

Zhang X G, Zhang T, Lin C Y et al. 2020. Reservoir architecture and evolution of meandering belt: a subsurface case in the Jiyang Depression, eastern China. *Journal of Petroleum Science and Engineering*, **193**: 107380, https://doi.org/10.1016/j.petrol.2020.107380.

Zhao R, Wang Q F, Liu X F et al. 2018. Uplift history of the Jiaodong Peninsula, eastern North China Craton: implications for lithosphere thinning and gold mineralization. *Geological Magazine*, **155**(4): 979-991, https://doi.org/10.1017/S0016756816001254.

Zhu X M, Liu Q H, Ge J W et al. 2019. Reconstruction of sediment-dispersal patterns using seismic sedimentology in the southeastern Zhanhua Sag, Bohai Bay Basin, China. *Journal of Petroleum Science and Engineering*, **182**: 106335, https://doi.org/10.1016/j.petrol.2019.106335.

Zhu X M, Zhang M Z, Zhu S F et al. 2022. Shale lithofacies and sedimentary environment of the third member, Shahejie Formation, Zhanhua Sag, Eastern China. *Acta Geologica Sinica*, **96**(3): 1024-1040, https://doi.org/10.1111/1755-6724.14804.